Uncertainty in aerosol radiative forcing impacts the simulated global monsoon in the 20th century

Jonathan K. P. Shonk[1], Andrew G. Turner[1, 2], Amulya Chevuturi[1], Laura J. Wilcox[1], Andrea J. Dittus[1] and Ed Hawkins[1]

[1]National Centre for Atmospheric Science, University of Reading, Reading, UK;

[2]Department of Meteorology, University of Reading, Reading, UK.

Corresponding author: Jonathan K. P. Shonk (j.k.p.shonk@reading.ac.uk)

Key Points:

- The impacts of the uncertainty in present-day aerosol radiative forcing on global monsoon rainfall are tested using historical simulations.
- Uncertainty in aerosol radiative forcing results in a difference of 2–3% in global monsoon area and intensity since 1950.
- Uncertainty in aerosol forcing translates to uncertainty in the sign of trends in global monsoon area and intensity between 1950 and 1980.

Abstract

Anthropogenic aerosols are dominant drivers of historical monsoon rainfall change. However, large uncertainties in the radiative forcing associated with anthropogenic aerosol emissions, and the dynamical response to this forcing, lead to uncertainty in the simulated monsoon response. We use historical simulations in which aerosol emissions are scaled by factors from 0.2 to 1.5 to explore the monsoon sensitivity to aerosol forcing uncertainty (-0.3 W m^{-2} to -1.6 W m^{-2}). Hemispheric asymmetry in emissions generates a strong relationship between scaling factor and both hemispheric temperature contrast and meridional location of tropical rainfall. Increasing the scaling from 0.2 to 1.5 reduces the global monsoon area by 3% and the global monsoon intensity by 2% over 1950–2014, and changes the dominant influence on the 1950–1980 monsoon rainfall trend from greenhouse gas to aerosol. Regionally, aerosol scaling has a pronounced effect on Northern Hemisphere monsoon rainfall.

Plain Language Summary

Greenhouse gas (GHG) and human-induced aerosol emissions have opposing effects on global monsoons, which supply water to billions of people: GHGs strengthen them; aerosols weaken them. This competition has been important in recent decades due to large aerosol emissions and will continue to be important in future until aerosol emissions are reduced.

Unfortunately, the effect of aerosols on global climate is very uncertain, leading to a range of temperature and rainfall patterns in model simulations of the last few decades and casting doubt on the magnitude of future climate change. Here, we investigate the effect of this uncertainty on monsoon rainfall using model simulations of the 20th century in which human-induced aerosol emissions are scaled by various factors, the range of which spans uncertainty in present-day aerosol radiative effect.

The uncertainty in the effects of human-induced aerosol emissions on global monsoon rainfall is profound. At its weakest, the impact of aerosol is overpowered by GHG and monsoon rainfall increases in the late 20th century. At its strongest, aerosol dominates over GHG, leading to reduced monsoon rainfall, particularly from 1950–1980. Our work emphasises the urgent need to reduce uncertainty in aerosol radiative effects to increase our confidence in future climate projections.

1 Background

Monsoon systems provide rainfall for billions of people, many of whom are dependent on the monsoon rains for survival. It is therefore important to understand the effects of climate change on the global monsoon, both in the past and future. Projections show a future increase in global monsoon area, rainfall amount and rainfall intensity (Hsu et al., 2012, 2013). In contrast, studies have reported a decline in global monsoon rainfall in the latter half of the 20th century (Hsu et al., 2011; Wang & Ding, 2006; Zhou et al., 2008). The decline is generally stronger in Northern Hemisphere (NH) monsoons (Zhou et al., 2008).

Bollasina et al. (2011), Polson et al. (2014), Salzmann et al. (2014) and Guo et al. (2015) have all shown that increasing emissions of anthropogenic aerosols (AA) and their precursors have played an important part in driving regional and global monsoon rainfall decrease during the mid-20th century. A key factor is the hemispheric asymmetry in AA emissions. In contrast to the global warming effect of greenhouse gas (GHG) emissions, AA emissions have a more regional impact and induce cooling, primarily in the NH, giving them a strong control on hemispheric temperature gradients (e.g., Wilcox et al., 2013). Changes to the hemispheric contrast in temperature have been shown to have profound effects on the climate system (Haywood et al., 2016; Stephens et al., 2016), including the strength of the Hadley circulation (Friedman et al., 2013) and location of the intertropical convergence zone (ITCZ; Broccoli et al., 2006; Voigt et al., 2017), both important elements of the monsoon systems. A weakening of the Hadley circulation was reported to be associated with the mid-20th-century reduction in monsoon rainfall (Guo et al., 2015; Polson et al., 2014), while a southward shift of the ITCZ was also identified (Allen et al., 2015; Hwang et al., 2013).

The observed reduction of Asian monsoon rainfall during the mid-20th century has been mainly attributed to the weakening Hadley circulation (Bollasina et al., 2011) and a reduction of available water vapour (Salzmann et al., 2014). However, local effects are also important: localised AA-induced cooling can oppose GHG-induced warming effects (Ramanathan et al., 2005; Ramanathan & Feng, 2009), leading to a slackening of temperature contrasts between land and sea via various mechanisms, resulting in weaker monsoon circulation (Lau & Kim, 2017). Remote aerosol emissions can also play a part in the changing monsoons – both Cowan and Cai (2011) and Dong et al. (2016) have shown that aerosols emitted remotely (outside the Asian region) can have similar magnitude impacts on the Asian summer monsoon to those emitted locally (albeit via different mechanisms).

In short, the impact of AA emissions on the global monsoon is a complex combination of local, remote and hemispheric effects, compounded by the heterogeneous distribution of emissions across the NH. In addition, there is also uncertainty in the total radiative effect of AA in the present day. According to the Intergovernmental Panel on Climate Change, present day top-of-atmosphere aerosol effective radiative forcing is -0.9 W m^{-2}, with a 5%-to-95% confidence interval spanning -1.9 W m^{-2} to -0.1 W m^{-2} (Myhre et al., 2013). Future reductions in AA emissions have the potential to cause increases in global precipitation comparable to those resulting from moderate GHG increases (Rotstayn et al., 2013), with the largest increases anticipated over East and South Asia (Levy et al., 2013; Westervelt et al., 2015). Rotstayn et al. (2013) found the magnitude of future precipitation increase to be correlated with historical effective radiative forcing. Uncertainty in the magnitude of aerosol forcing, and the monsoon response to it, is compounded in climate projections, where potential aerosol emission pathways are diverse. In the Asian region in particular, there is great variety in future emission trends across the Shared Socio-Economic Pathways (Samset et al., 2019).

In this study, we quantify the effects of the uncertainty in aerosol radiative forcing on the global monsoon system using a set of simulations produced as part of the SMURPHS ("Securing Multidisciplinary Understanding and Prediction of Hiatus and Surge Events") project (Dittus et al., 2019). The SMURPHS ensemble consists of a set of historical climate simulations with AA emissions scaled by various factors, allowing us for the first time to investigate the sensitivity of the climate system to the strength of the forcing in a single climate model without structural or parametric uncertainty arising from the use of single-forcing simulations from a multi-model ensemble (such as the AA-only simulations from CMIP5; Taylor et al., 2012). We introduce the ensemble and experimental design in more detail in Section 2. The effect of the aerosol scaling in terms of temperature contrasts across hemispheres, and between land and sea, is examined in Section 3. Section 4 presents the effects of scaling on standard metrics of the global and regional monsoons. We summarise and conclude in Section 5.

2 SMURPHS ensemble and aerosol emission data

The SMURPHS dataset consists of historical climate simulations run over the period 1850–2014 using a fully coupled version of HadGEM3-GC3.1 at resolutions of N96 and 1° in the atmosphere and ocean respectively (Kuhlbrodt et al., 2018; Williams et al., 2018). The model version used here is a development version towards the UK submission to CMIP6 (Dittus et al, 2019; Hardiman et al., 2019). Four ensemble members are run for each of five experiments in which the historical aerosol emissions are scaled by a constant factor. This factor is applied to emissions of all species of anthropogenic aerosol and precursors, and at all locations throughout the historical emissions dataset. Five scaling factors were selected: ×0.2, ×0.4, ×0.7, ×1.0 and ×1.5, with the ×1.0 scaling corresponding to the standard CMIP6 historical protocol. The scaling factors have been chosen to span the range of uncertainty in present-day aerosol radiative forcing according to Myhre et al. (2013), with the ×0.2 scaling corresponding to a forcing of -0.35 W m^{-2} and the ×1.5 scaling corresponding to a forcing of -1.6 W m^{-2}. More detail on the SMURPHS ensemble is presented by Dittus et al. (2019).

The SMURPHS simulations use the same aerosol emission dataset as CMIP6 (Hoesly et al., 2018), which contains emissions data from 1750–2014 for sulphur dioxide, black carbon and organic carbon. Emissions from 1900 onwards are shown in Figure 1. In the early 20th century, emissions increase gradually, but then ramp up from 1950 to 1980. Since 1980, emission mitigation efforts in North America and Europe have been balanced by continued increases in Asia, causing global emissions to level off. The hemispheric asymmetry in AA emissions is clear, with the NH contributing approximately 90% of the global total throughout the 20th century (Figures 1b, 1c). Most monsoon regions show a gradual increase in emissions in the 20th century, with pronounced increases since 1970 in the Indian and East Asian sectors (Figures 1g, 1h).

In this study, we use all four members from each of the five experiments, but include years from 1900 onwards, to allow 50 years for the model to adjust to the scalings (after Dittus et al., 2019). When considering climatological quantities, we consider the ensemble mean for each experiment to be the model estimate of the climate system under those scaling conditions and indicate uncertainty across ensemble members in terms of inter-member standard deviation. Where quantities are averaged over areas, a cosine-based latitude weighting is applied.

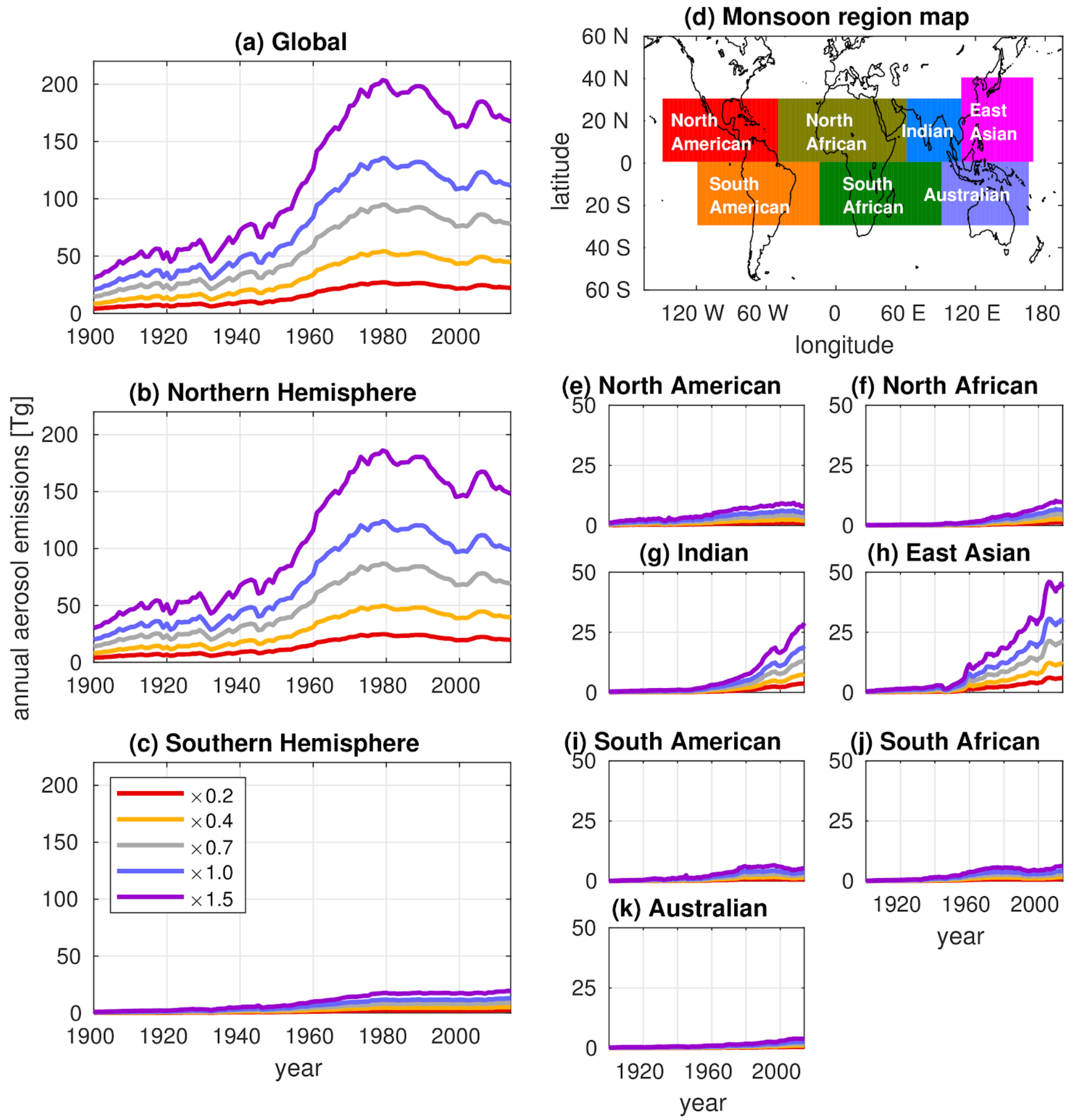

Figure 1. Sulphur dioxide emissions used in SMURPHS on (**a**) global, (**b**, **c**) hemispheric and (**e–k**) regional scales, in Tg yr^{-1}. Organic and black carbon emissions are scaled in the same way. Monsoon regions are as defined in panel (**d**).

3 Temperatures and contrasts

The effect of AA on global mean temperature is clear (Figure 2a). Higher aerosol scalings lead to cooler global temperatures, and by the 1970–2014 period there is little overlap in global temperature between scalings. We also see evidence of the control by AA emissions on the mid-20th-century hiatus (the period 1950–1980), in agreement with the findings of Wilcox et al. (2013) and Jones et al. (2013). The higher scalings lead to a stronger hiatus; the lower scalings lead to a much weaker hiatus. In the ×0.2 experiment, a hiatus is barely discernible. These results echo those of Dittus et al. (2019).

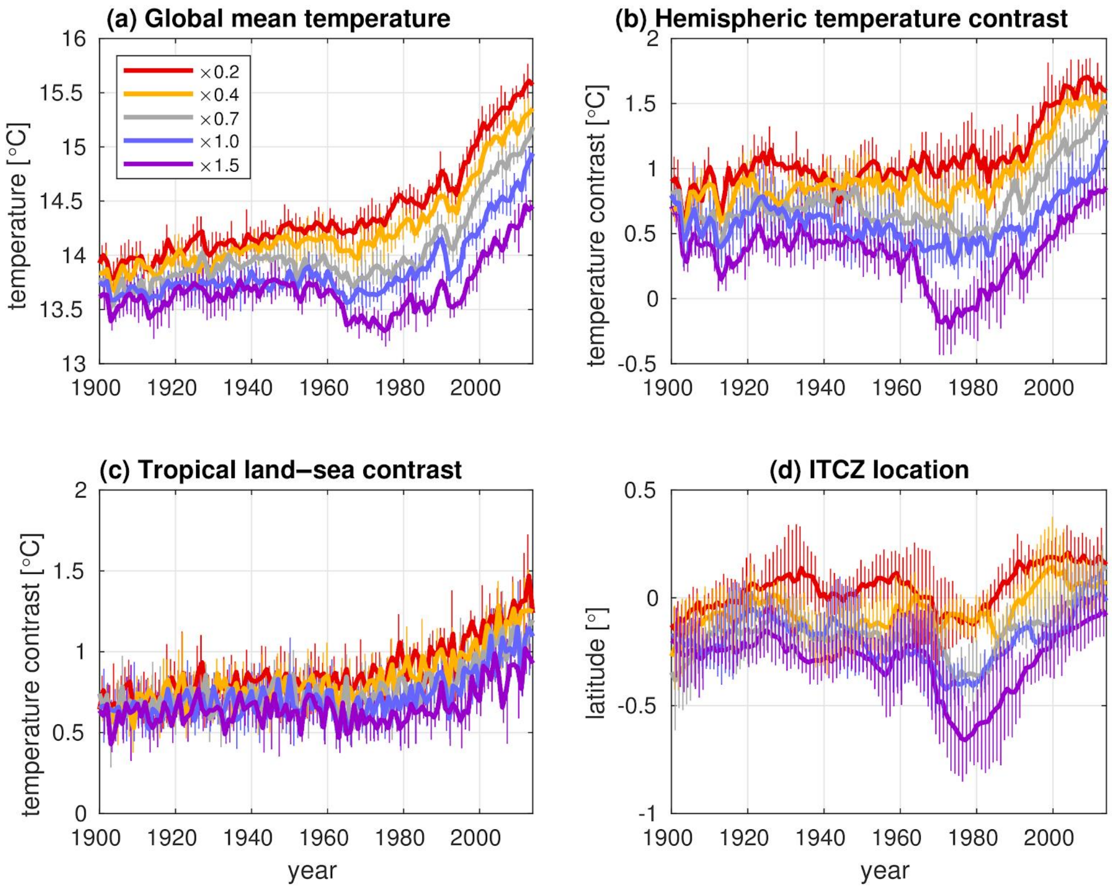

Figure 2. Time series of various atmospheric properties from the SMURPHS simulations: (**a**) global mean surface air temperature; (**b**) hemispheric temperature contrast (NH minus SH); (**c**) tropical land–sea temperature contrast, calculated in the summer months (November–March in SH, May–September in NH) for latitudes within 30° S and 30° N only; (**d**) global mean ITCZ location, calculated following **Shonk et al. (2018)**. All values are ensemble means; vertical error bars indicate one standard deviation across the four ensemble members.

The hemispheric asymmetry of AA emissions leads to a much greater degree of cooling in the NH, so the strength of the forcing has a control on the hemispheric temperature contrast (HTC), defined NH minus SH (Chang et al., 2011; Wilcox et al., 2013). Lower scalings reduce the degree of NH cooling and therefore increase the HTC (Figure 2b). The NH is, on average, warmer than the southern hemisphere (SH; for example, Kang et al., 2015) although, under the highest scaling (×1.5), the HTC reverses in sign during the 1970s and 1980s.

This shift in HTC is reflected in the location of the ITCZ. We calculate ITCZ location using the method of Shonk et al. (2018), the ITCZ at a given longitude being defined as the latitude centroid of the region of rainfall that exceeds 50% of the maximum value at that longitude. The ITCZ location presented here (Figure 2d) is the zonal mean value (note that the general location of the ITCZ south of the equator is caused by the inclusion of the Southern Pacific and Atlantic Convergence Zones). Lower scalings, associated with a warmer NH and stronger HTC, lead to an ITCZ location that is further north, consistent with Hwang et al. (2013), Allen et al. (2015) and Chung and Soden (2017).

Table 1. Mean monsoon-related properties, as defined in Sections 3 and 4, averaged over the period 1950 to 2014 (during which global aerosol emissions increased), and all four ensemble members. The difference column is the change from ×0.2 (lowest scaling) to ×1.5 (highest scaling), expressed as a percentage where indicated.

	×0.2	**×0.4**	**×0.7**	**×1.0**	**×1.5**	**Difference**
Global mean temperature [°C]	14.65	14.45	14.18	13.99	13.71	**−0.94**
Hemispheric temperature contrast [°C]	1.19	1.03	0.78	0.58	0.29	**−0.91**
ITCZ location (latitude) [°]	0.07	−0.03	−0.16	−0.23	−0.34	**−0.40**
Tropical land–sea contrast [°C]	0.98	0.91	0.82	0.77	0.68	**−0.30**
GMA [Mm^2]	126.7	126.0	125.0	124.5	122.8	**−3.04%**
HMA (NH) [Mm^2]	66.7	66.0	65.5	65.0	63.9	**−4.23%**
HMA (SH) [Mm^2]	60.0	59.9	59.5	59.6	59.0	**−1.72%**
GMI [mm d^{-1}]	7.77	7.74	7.68	7.66	7.61	**−2.01%**
HMI (NH) [mm d^{-1}]	7.69	7.65	7.56	7.54	7.48	**−2.78%**
HMI (SH) [mm d^{-1}]	7.86	7.84	7.81	7.78	7.76	**−1.24%**

Monsoon strength is also influenced by changes in the land–sea temperature contrast (LSTC), both on regional (Lau & Kim, 2017) and global (Fasullo, 2012) scales. While weaker than the effect on HTC, there is a degree of control of the aerosol scaling on the LSTC, albeit with a larger overlap between ensemble members (Figure 2c). Higher scalings result in cooler land surfaces with respect to the surrounding oceans, hence the LSTC is reduced, and the monsoon is weakened.

The control of the aerosol forcing on the properties presented in this section is demonstrated quantitatively in the top section of Table 1 in terms of means over the 1950–2014 period, when most changes in anthropogenic aerosol have occurred. All properties vary monotonically and roughly linearly across the range of scalings used in SMURPHS, with higher scalings resulting in a cooler global temperature, a weaker HTC, an ITCZ situated further south, and a weaker LSTC. The impact of the uncertainty in present-day forcing on these properties is presented in the rightmost column of Table 1 as the differences between the lowest and highest scalings (×1.5 minus ×0.2). Changing the forcing from lowest to highest value lowers global temperature by nearly 1 °C and reduces the HTC from 1.19 °C to 0.29 °C. The zonal-mean ITCZ location shifts southwards by 0.40° of latitude, and the LSTC reduces by just over 30%, from 0.95 °C to 0.65 °C.

4 Monsoon area and rainfall

We evaluate the effects of aerosol scaling on the monsoon via Global Monsoon Area (GMA) and Global Monsoon Intensity (GMI). These properties are defined following Liu et al. (2009), Hsu et al. (2011) and others: a gridbox is within the GMA if the difference in summer and winter rainfall (May to September and November to March, depending on hemisphere) is greater than 2 mm d^{-1}, and more than 55% of the rain falls in the summer months. The total GMA is calculated as the sum of the area of all gridboxes within the GMA region. GMI is then calculated as the total rainfall within the GMA, divided by the area of the GMA. We also define hemispheric equivalents (HMA and HMI) – these are the GMA and GMI calculated separately for each hemisphere.

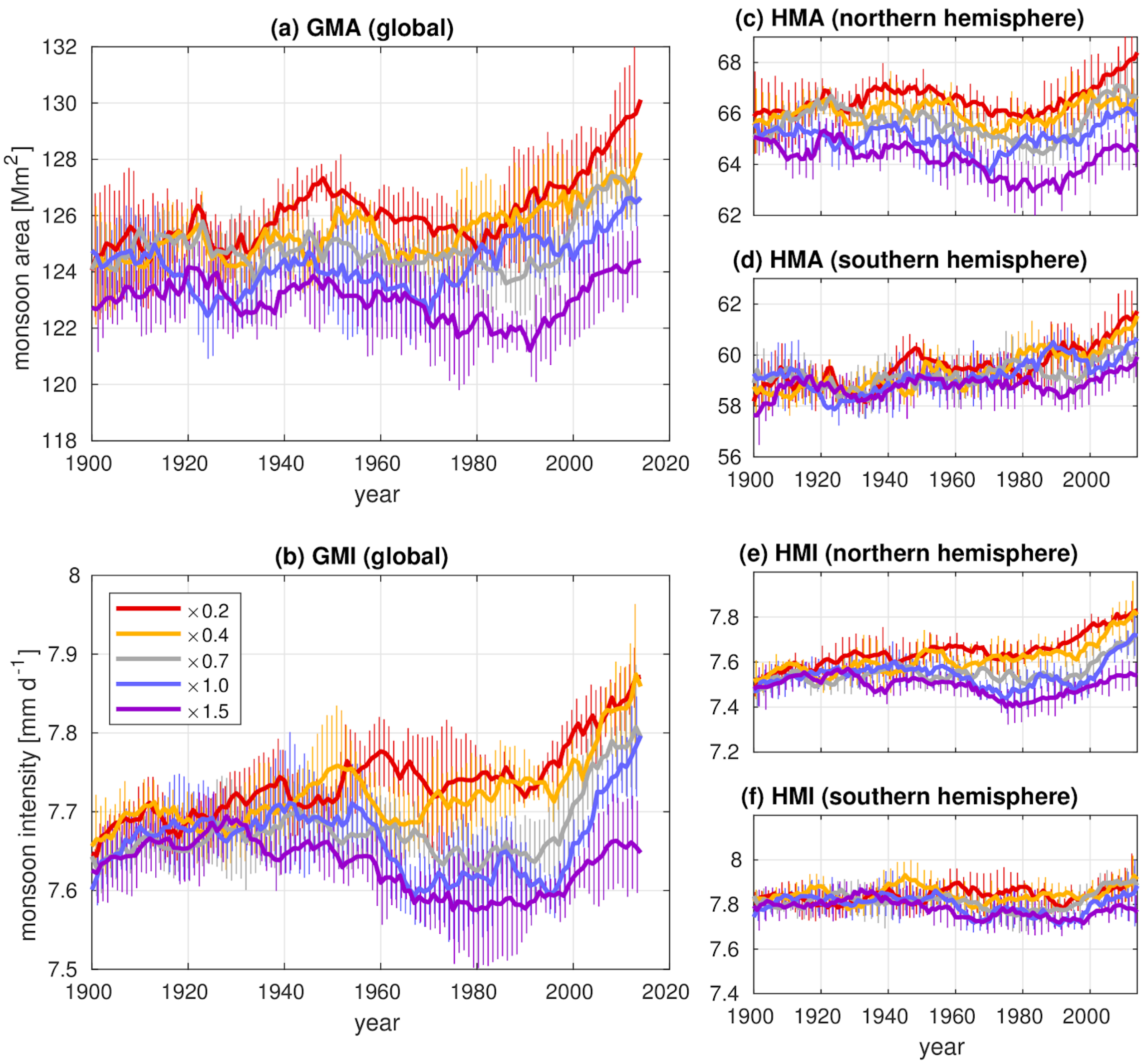

Figure 3. Time series of (**a**) global monsoon area (GMA) and (**b**) global monsoon intensity (GMI) for each experiment. Panels (**c**, **d**) and (**e**, **f**) show the hemispheric equivalents (HMA and HMI) for NH and SH. The ensemble mean is shown, with an 11-year running mean applied. The vertical error bars indicate the standard deviation across the four members. GMA is in Mm^2, where 1 Mm^2 = 1 × 10^6 km^2.

Both GMA and GMI show a dependence on AA forcing (Figures 3a, 3b), with a higher scaling leading to a reduction of both intensity and area. This is consistent with the effects of the scaling on global temperature, HTC and LSTC, which are also reduced at higher scalings. This dependence is clearest in GMI from 1950–1980: during this period, higher scalings produce a greater weakening of the GMI than lower scalings. This suggests a switch between GHGs and AAs dominating the influence on the monsoon from 1950–1980 across the range of uncertainty in aerosol forcing. The dependence is also clear in GMA, although the timing, duration, and strength of the GMA reduction after 1950 vary across scalings. This is most likely associated with natural variability across the four ensemble members.

Despite this variability, the effect of the scalings on GMA and GMI when averaged over 1950–2014 is also monotonic and roughly linear with scaling factor across the experiments (Table 1). The effect of the uncertainty in aerosol radiative forcing on GMA and GMI is a reduction of 3.0% and 2.0% respectively, when increasing the scaling across its range. For context, Hsu et al. (2013) found that 1 °C of warming in CMIP5 models resulted in multi-model mean increases of 1.9% and 1.3% in GMA and GMI (see their Figure 5). The sensitivities identified here are higher (about 3.3% and 2.1% per °C), although lie well within the range of sensitivities presented by Hsu et al. (2013).

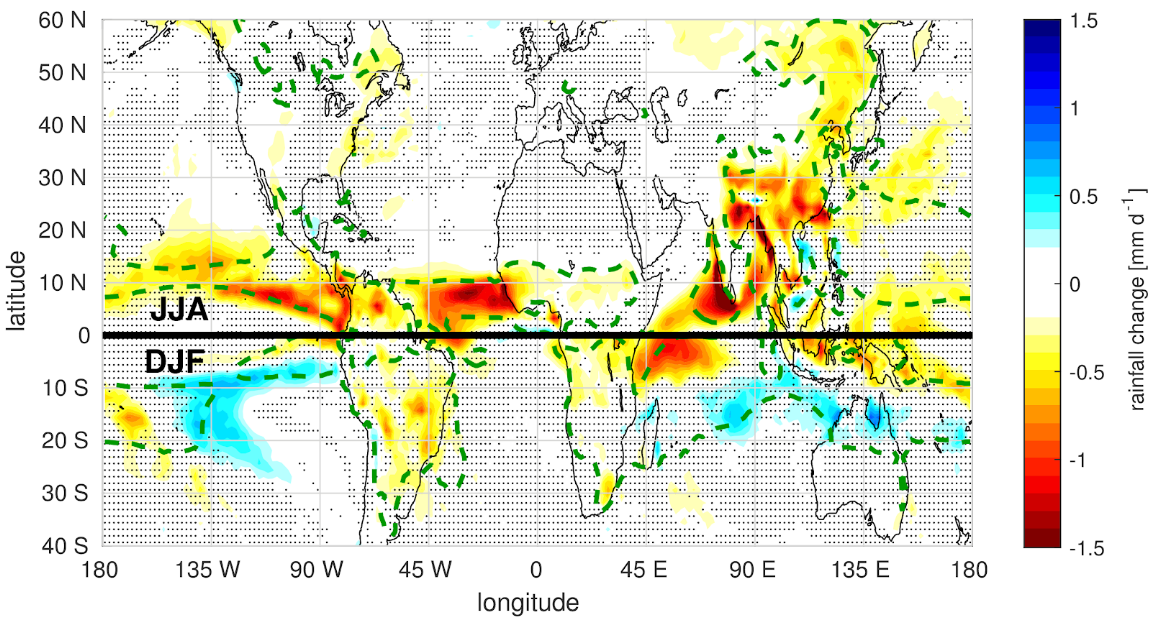

Figure 4. The difference in monsoon rainfall (in mm d^{-1}) across the range of the scaling factors (×1.5 minus ×0.2). The summer months are shown in each hemisphere (June–August in the NH, December–February in the SH); the thick black line marks the equator. Averaged over the period 1950–2014, and across all ensemble members. The green dotted line indicates the mean GMA in the ×1.0 experiment. Spots indicate regions where the rainfall difference is insignificant with respect to variability across years and members.

The effects of aerosol scaling on both GMA and GMI are dominated by the NH, with a weak dependence on the scaling found in the SH (Figures 3c–3f). The effect of uncertainty in aerosol radiative forcing has substantial effects on the rainfall in the regional monsoons (Figure 4), with the greatest rainfall changes in the NH monsoons. The North American and North African monsoon experience a marked reduction, while the decrease in the Asian monsoon is even greater (consistent with the much larger aerosol emissions originating there; see Figures 1g, 1h).

The effect of the scaling on the SH monsoons, in contrast, is much more variable, reflecting the much smaller aerosol forcing there. The effect of the aerosol forcing uncertainty on HMA and HMI from 1950 onwards in the NH is more than twice that in the SH (Table 1).

5 Summary and conclusions

The observed reduction in global monsoon area and intensity since 1950 has been widely attributed to a rapid increase in emissions of anthropogenic aerosols and their precursors. The cooling associated with these emissions is concentrated in the Northern Hemisphere, and opposes the warming effect of greenhouse gases and reduces the temperature contrast between hemispheres and between land and sea. This has been shown to weaken the monsoon circulations, resulting in a reduction of monsoon rainfall. Understanding the interplay between aerosol forcing and monsoon properties in past simulations is important in order to constrain future monsoon projections, where anthropogenic aerosol reductions are likely to strengthen the monsoon, in addition to the strengthening anticipated in response to further increases in greenhouse gases.

We explored the sensitivity of the global monsoon to uncertainty in aerosol radiative forcing using an ensemble of historical simulations in which anthropogenic aerosol and precursor emissions from 1850–2014 are scaled by factors ranging from ×0.2 to ×1.5 (corresponding to a present-day aerosol effective radiative forcing range of -0.35 W m^{-2} to -1.6 W m^{-2}). When averaged over 1950–2014, increasing the scaling factor across this range results in a 0.94 °C cooling of global temperature, a 75% reduction in hemispheric temperature contrast, a 30% reduction in land–sea temperature contrast, and a southward shift of the ITCZ by 0.4° of latitude. The global monsoon area is reduced by 3% and the intensity of the rainfall within this region is reduced by 2%. Regionally, much of the reduction in monsoon area and intensity arises in the Northern Hemisphere monsoons, particularly the Asian sector, where emission changes are greatest.

Long-term monsoon variability since 1950 has very different characteristics across the scaling factors. In the ×1.5 experiment, an overall negative trend in monsoon rainfall intensity is found, dominated by strong aerosol forcing; in the ×0.2 experiment, greenhouse gases are able to dominate and monsoon intensity increases. Reducing uncertainty in the radiative forcing associated with anthropogenic aerosol would provide more reliable estimates of the future evolution of global and regional monsoons as anthropogenic aerosol and precursor emissions decline.

Acknowledgements

This work was funded by the SMURPHS, REAL Projections, and EMERGENCE projects under the Natural Environment Research Council (NERC; Grants NE/N006054/1, NE/N018591/1, and NE/S004890/1 respectively). EH and the SMURPHS ensemble were additionally supported by the National Centre for Atmospheric Science. AC was supported by the Climate Science for Services Partnership (CSSP) China project funded by the Newton Fund. We acknowledge the use of the Monsoon2 system, a collaborative facility supplied under the Joint Weather and Climate Research Programme, a strategic partnership between the UK Met Office and NERC.

The data are currently being archived at the UK Centre for Environmental Data Analysis and will be available by the publication date. All authors declare that they have no conflicts of interest.

References

Allen, R. J., Evan, A. T., & Booth, B. B. B. (2015). Interhemispheric aerosol radiative forcing and tropical precipitation shifts during the late twentieth century. *Journal of Climate* 28: 8219—8246, https://doi.org/10.1175/jcli-d-15-0148.1

Bollasina, M. A., Ming, Y., & Ramaswamy, V. (2011). Anthropogenic aerosols and the weakening of the South Asian summer monsoon. *Science* 334, 502—505, https://doi.org/10.1126/science.1204994

Broccoli, A. J., Dahl, K. A., & Stouffer, R. J. (2006). Response of the ITCZ to northern hemisphere cooling. *Geophysical Research Letters* 33, L01702, https://doi.org/10.1029/2005gl024546

Chang, C. Y., Chiang, J. C. H., Wehner, M. F., Friedman, A. R., & Ruedy, R. (2011). Sulphate aerosol control of tropical Atlantic climate over the twentieth century. *Journal of Climate* 24, 2540—2555, https://doi.org/10.1175/2010jcli4065.1

Chung, E.-S., & Soden, B. J. (2017). Hemispheric climate shifts driven by anthropogenic aerosol–cloud interactions. *Nature Geoscience* 10, 566—571, https://doi.org/10.1038/ngeo2988

Cowan, T., & Cai, W. (2011). The impact of Asian and non-Asian anthropogenic aerosols on 20th century Asian summer monsoon. *Geophysical Research Letters* 38, L11703, https://doi.org/10.1029/2011gl047268

Dong, B., Sutton, R. T., Highwood, E. J., & Wilcox, L. J. (2016). Preferred response of the East Asian summer monsoon to local and non-local anthropogenic sulphur dioxide emissions. *Climate Dynamics* 46, 1733—1751, https://doi.org/10.1007/s00382-015-2671-5

Dittus, A. J., Hawkins, E., Wilcox, L. J., Sutton, R. T., Smith, C. J., Andrews, M. B., & Forster, P. M. (2019). Sensitivity of historic climate simulations to uncertain aerosol forcing. Submitted to *Geophysical Research Letters*: manuscript 2019GL085806.

Fasullo, J. (2012). A mechanism for land–ocean contrasts in global monsoon trends in a warming climate. *Climate Dynamics* 39, 1137—1147, https://doi.org/10.1007/s00382-011-1270-3

Friedman, A. R., Hwang, Y. T., Chiang, J. C. H., & Frierson, D. M. W. (2013). Interhemispheric temperature asymmetry over the twentieth century and in future projections. *Journal of Climate* 26, 5419—5433, https://doi.org/10.1175/jcli-d-12-00525.1

Guo, L., Turner, A. G., & Highwood, E. J. (2015). Impacts of 20th century aerosol emissions on the South Asian monsoon in the CMIP5 models. *Atmospheric Chemistry and Physics* 15, 6367—6378, https://doi.org/10.5194/acp-15-6367-2015

Hardiman, S. C., Andrews, M. B., Andrews, T., Bushell, A. C., Dunstone, N. J., Dyson, H., et al. (2019). The impact of prescribed ozone in climate projections run with HadGEM3-GC3.1. *Journal of Advances in Modelling Earth Systems* 11, https://doi.org/10.1029/2019MS001714

Haywood, J. M., Jones, A., Dunstone, N., Milton, S., Vellinga, M., Bodas-Salcedo, A., et al. (2016). The impact of equilibriating hemispheric albedos on tropical performance in the HadGEM2-ES coupled climate model. *Geophysical Research Letters* 43, 395—403, https://doi.org/10.1002/2015gl066903

Hoesly, R. M., Smith, S. J., Feng, L., Klimont, Z., Janssens-Maenhout, G., Pitkanen, T., et al. (2018). Historical (1750–2014) anthropogenic emissions of reactive gases and aerosols from the Community Emissions Data System (CEDS). *Geoscientific Model Development* 11, 369—408, https://doi.org/10.5194/gmd-11-369-2018

Hsu, P. C., Li, T., Luo, J. J., Murakami, H., Kitoh, A., & Zhao, M. (2012). Increase of global monsoon area and precipitation under global warming: a robust signal? *Geophysical Research Letters* 39, L06701, https://doi.org/10.1029/2012gl051037

Hsu, P. C., Li, T., Murakami, H., & Kitoh, A. (2013). Future change of the global monsoon revealed from 19 CMIP5 models. *Journal of Geophysical Research: Atmospheres* 118, 1237—1260, https://doi.org/10.1002/jgrd.50145

Hsu, P. C., Li, T., & Wang, B. (2011). Trends in global monsoon area and precipitation over the past 30 years. *Geophysical Research Letters* 38, L08701, https://doi.org/10.1029/2011gl046893

Hwang, Y. T., Frierson, D. M. W., & Kang, S. M. (2013). Anthropogenic sulphate aerosol and the southward shift of tropical precipitation in the late 20th century. *Geophysical Research Letters* 40, 2845—2850, https://doi.org/10.1002/grl.50502

Jones, G. S., Stott, P. A., & Christidis, N. (2013). Attribution of observed historical near-surface temperature variations to anthropogenic and natural causes using CMIP5 simulations. *Journal of Geophysical Research: Atmospheres* 118, 4001—4024, https://doi.org/10.1002/jgrd.50239.

Kang, S. M., Seager, R., Frierson, D. M. W., & Liu, X. (2015). Croll revisited: why is the northern hemisphere warmer than the southern hemisphere? *Climate Dynamics* 44, 1457—1472, https://doi.org/10.1007/s00382-014-2147-z

Kuhlbrodt, T., Jones, C. G., Sellar, A., Storkey, D., Blockley, E., Stringer, M., et al. (2018). The low-resolution version of HadGEM3 GC3.1: development and evaluation for global climate. *Journal of Advances in Modelling Earth Systems* 10, 2865—2888, https://doi.org/10.1029/2018ms001370

Lau, W. K. M., & Kim, K. M. (2017). Competing influences of greenhouse warming and aerosols on Asian summer monsoon circulation and rainfall. *Asia-Pacific Journal of Atmospheric Sciences* 53, 181—194, https://doi.org/10.1007/s13143-017-0033-4

Levy II, H., Horowitz, L. W., Schwarzkopf, M. D., Ming, Y., Gloaz, J.-C., Naik, V., & Ramaswamy, V. (2013). The roles of aerosol direct and indirect effects in past and future climate change. *Journal of Geophysical Research: Atmospheres* 118, 4521—4532, https://doi.org/10.1002/jgrd.50192.

Liu, J., Wang, B., Ding, Q., Kuang, X., Soon, W., & Zorita, E. (2009). Centennial variations of the global monsoon precipitation in the last millennium: results from ECHO-G model. *Journal of Climate* 22, 2356—2371, https://doi.org/10.1175/2008jcli2353.1

Myhre, G., Shindell, D., Bréon, F. M., Collins, W., Fuglestvedt, J., Huang, J., et al. (2013). *Anthropogenic and Natural Radiative Forcing* – in *Climate Change 2013: the Physical Science Basis*. Contribution of Working Group I to the Fifth Assessment Report of the Intergovernmental Panel on Climate Change. Cambridge University Press, https://doi.org/10.1017/CBO9781107415324

Polson, D., Bollasina, M., Hegerl, G. C., & Wilcox, L. J. (2014). Decreased monsoon precipitation in the northern hemisphere due to anthropogenic aerosols. *Geophysical Research Letters* 41, 6023—6029, https://doi.org/10.1002/2014gl060811

Ramanathan, V., Chung, C., Kim, D., Bettge, T., Buja, L., Kiehl, J. T., et al. (2005). Atmospheric brown clouds: impacts on South Asian climate and hydrological cycle. *Proceedings of the National Academy of Sciences* 102, 5326—5333, https://doi.org/10.1073/pnas.0500656102

Ramanathan, V., & Feng, Y. (2009). Air pollution, greenhouse gases and climate change: global and regional perspectives. *Atmospheric Environment* 43, 37—50, https://doi.org/10.1016/j.atmosenv.2008.09.063

Rotstayn, L. D., Collier, M. A., Chrastansky, A., Jeffrey, S. J., & Luo, J.-J. (2013). Projected effects of declining aerosols in RCP4.5: unmasking global warming? *Atmospheric Chemistry and Physics* 13, 10883—10905. https://doi.org/ 10.5194/acp-13-10883-2013.

Salzmann, M., Weser, H., & Cherian, R. (2014). Robust response of Asian summer monsoon to anthropogenic aerosols in CMIP5 models. *Journal of Geophysical Research: Atmospheres* 119, 11321—11337, https://doi.org/10.1002/2014jd021783

Samset, B. H., Lund, M. T., Bollasina, M., Myhre, G., & Wilcox, L. J. (2019). Emerging Asian aerosol patterns. *Nature Geoscience* 12, 582—586, https://doi.org/10.1038/s41561-019-0424-5

Shonk, J. K. P., Guilyardi, E., Toniazzo, T., Woolnough, S. J., & Stockdale, T. (2018). Identifying causes of western Pacific ITCZ drift in ECMWF System 4 hindcasts. *Climate Dynamics* 50, 939—954, https://doi.org/10.1007/s00382-017-3650-9

Stephens, G. L., Hakuba, M. Z., Hawcroft, M., Haywood, J. M., Behrangi, A., Kay, J. E., & Webster, P. J. (2016). The curious nature of the hemispheric symmetry of the Earth's water and energy balances. *Current Climate Change Reports* 2, 135—147, https://doi.org/10.1007/s40641-016-0043-9

Taylor, K. E., Stouffer, R. J., & Meehl, G. A. (2012). An overview of CMIP5 and the experiment design. *Bulletin of the American Meteorological Society* 93, 485—498, https://doi.org/10.1175/bams-d-11-00094.1

Voigt, A., Pincus, R., Stevens, B., Bony, S., Boucher, O., Bellouin, N., et al. (2017). Fast and slow shifts of the zonal-mean intertropical convergence zone in response to an idealised anthropogenic aerosol. *Journal of Advances in Modelling Earth Systems* 9, 870—892, https://doi.org/10.1002/2016ms000902

Wang, B., & Ding, Q. (2006). Changes in global monsoon precipitation over the past 56 years. *Geophysical Research Letters* 33, L06711, https://doi.org/10.1029/2005gl025347

Westervelt, D. M., Horowitz, L. W., Naik, V., Golaz, J.-C., & Mauzerall, D. L. (2015). Radiative Forcing and Climate Response to Projected 21st Century Aerosol Decreases. *Atmospheric Chemistry and Physics* 15, 12681—12703, https://doi.org/10.5194/acp-15-12681-2015

Wilcox, L. J., Highwood, E. J., & Dunstone, N. J. (2013). The influence of anthropogenic aerosol on multi-decadal variations of historical global climate. *Environmental Research Letters* 8, 024033, https://doi.org/10.1088/1748-9326/8/2/024033

Williams, K. D., Copsey, D., Blockley, E. W., Bodas-Salcedo, A., Calvert, D., Comer, R., et al. (2018). The Met Office Global Coupled Model 3.0 and 3.1 (GC3.0 and GC3.1) configurations. *Journal of Advances in Modelling Earth Systems* 10, 357—380, https://doi.org/10.1002/2017MS001115

Zhou, T., Zhang, L., & Li, H. (2008). Changes in global land monsoon area and total rainfall accumulation over the last half century. *Geophysical Research Letters* 35, L16707, https://doi.org/10.1029/2008gl034881